

# Nonlinear silicon nitride waveguides based on a PECVD deposition platform

LINGHUA WANG,<sup>1,4,\*</sup> WEIQIANG XIE,<sup>2,4</sup> DRIES VAN THOURHOUT,<sup>2</sup> YAZHEN ZHANG,<sup>1</sup> HUI YU,<sup>3</sup> AND SHAOHAO WANG<sup>1</sup>

<sup>1</sup>College of Physics and Information Engineering, Fuzhou University, Fuzhou, 350116, China

<sup>2</sup>Photonics Research Group, Department of Information Technology, Ghent University-IMEC, Gent B-9000, Belgium

<sup>3</sup>Department of Information Science and Electronics Engineering, Zhejiang University, Hangzhou 310027, China

<sup>4</sup>Contributed equally to this work

\*wangling\_hua@sina.com

**Abstract:** In this work, we present a nonlinear silicon nitride waveguide. These waveguide are fabricated by readily available PECVD, conventional contact UV-lithography and high-temperature annealing techniques, thus dramatically reducing the processing complexity and cost. By patterning the waveguide structures firstly and then carrying out a high-temperature annealing process, not only sufficient waveguide thickness can be achieved, which gives more freedom to waveguide dispersion control, but also the material absorption loss in the waveguides be greatly reduced. The linear optical loss of the fabricated waveguide with a cross-section of  $2.0 \times 0.58 \mu\text{m}^2$  was measured to be as low as 0.58 dB/cm. The same loss level is demonstrated over a broad wavelength range from 1500 nm to 1630 nm. Moreover, the nonlinear refractive index of the waveguide was determined to be  $\sim 6.94 \times 10^{-19} \text{ m}^2/\text{W}$ , indicating that comparable nonlinear performance with their LPCVD counterparts is expected. These silicon nitride waveguides based on a PECVD deposition platform can be useful for the development of more complicated on-chip nonlinear optical devices or circuits.

© 2018 Optical Society of America under the terms of the [OSA Open Access Publishing Agreement](#)

**OCIS codes:** (190.4380) Nonlinear optics, four-wave mixing; (220.0220) Optical design and fabrication; (230.7370) Waveguides.

## References and links

1. D. J. Moss, R. Morandotti, A. L. Gaeta, and M. Lipson, "New CMOS-compatible platforms based on silicon nitride and Hydex for nonlinear optics," *Nat. Photonics* **7**(8), 597–607 (2013).
2. T. Ning, H. Pietarinen, O. Hyvärinen, J. Simonen, G. Genty, and M. Kauranen, "Strong second-harmonic generation in silicon nitride films," *Appl. Phys. Lett.* **100**(16), 161902 (2012).
3. K. Ikeda, R. E. Saperstein, N. Alic, and Y. Fainman, "Thermal and Kerr nonlinear properties of plasma-deposited silicon nitride/ silicon dioxide waveguides," *Opt. Express* **16**(17), 12987–12994 (2008).
4. D. T. H. Tan, K. Ikeda, P. C. Sun, and Y. Fainman, "Group velocity dispersion and self phase modulation in silicon nitride waveguides," *Appl. Phys. Lett.* **96**(6), 061101 (2010).
5. R. Baets, A. Z. Subramanian, S. Clemmen, B. Kuyken, P. Bienstman, N. Le Thomas, G. Roelkens, D. Van Thourhout, P. Helin, and S. Severi, "Silicon photonics: silicon nitride versus silicon-on-insulator" *Proc. Optical Fiber Communication. Conference (OFC), Th3J.1*, (2016).
6. A. Rahim, E. Ryckeboer, A. Z. Subramanian, S. Clemmen, B. Kuyken, A. Dhakal, A. Raza, A. Hermans, M. Muneeb, S. Dhoore, Y. Li, U. Dave, P. Bienstman, N. L. Thomas, G. Roelkens, D. V. Thourhout, P. Helin, S. Severi, X. Rottenberg, and R. Baets, "Expanding the Silicon Photonics Portfolio With Silicon Nitride Photonic Integrated Circuits," *J. Lightwave Technol.* **35**(4), 639–649 (2017).
7. C. J. Krückel, A. Fülöp, Z. Ye, P. A. Andrekson, and V. Torres-Company, "Optical bandgap engineering in nonlinear silicon nitride waveguides," *Opt. Express* **25**(13), 15370–15380 (2017).
8. C. Lacava, S. Stankovic, A. Z. Khokhar, T. D. Bucio, F. Y. Gardes, G. T. Reed, D. J. Richardson, and P. Petropoulos, "Si-rich silicon nitride for nonlinear signal processing applications," *Sci. Rep.* **7**(1), 22 (2017).
9. T. Ning, O. Hyvärinen, H. Pietarinen, T. Kaplas, M. Kauranen, and G. Genty, "Third-harmonic UV generation in silicon nitride nanostructures," *Opt. Express* **21**(2), 2012–2017 (2013).
10. J. F. Bauters, M. J. R. Heck, D. John, D. Dai, M.-C. Tien, J. S. Barton, A. Leinse, R. G. Heideman, D. J. Blumenthal, and J. E. Bowers, "Ultra-low-loss high-aspect-ratio  $\text{Si}_3\text{N}_4$  waveguides," *Opt. Express* **19**(4), 3163–3174 (2011).

11. G.-R. Lin, S.-P. Su, C.-L. Wu, Y.-H. Lin, B.-J. Huang, H.-Y. Wang, C.-T. Tsai, C.-I. Wu, and Y.-C. Chi, "Si-rich SiN<sub>x</sub> based Kerr switch enables optical data conversion up to 12 Gbit/s," *Sci. Rep.* **5**(9611), 9611 (2015).
12. Y. Okawachi, K. Saha, J. S. Levy, Y. H. Wen, M. Lipson, and A. L. Gaeta, "Octave-spanning frequency comb generation in a silicon nitride chip," *Opt. Lett.* **36**(17), 3398–3400 (2011).
13. T. Wang, D. K. T. Ng, S. K. Ng, Y. T. Toh, A. K. L. Chee, G. F. R. Chen, Q. Wang, and D. T. H. Tan, "Supercontinuum generation in bandgap engineered, back-end CMOS compatible silicon rich nitride waveguides," *Laser Photonics Rev.* **9**(5), 498–506 (2015).
14. K. Luke, A. Dutt, C. B. Poitras, and M. Lipson, "Overcoming Si<sub>3</sub>N<sub>4</sub> film stress limitations for high quality factor ring resonators," *Opt. Express* **21**(19), 22829–22833 (2013).
15. Y. Xuan, Y. Liu, L. T. Varghese, A. J. Metcalf, X. Xue, P.-H. Wang, K. Han, J. A. Jaramillo-Villegas, A. Al Noman, C. Wang, S. Kim, Y. J. Lee, B. Niu, L. Fan, J. Wang, D. E. Leaird, A. M. Weiner, and M. Qi, "High-Q silicon nitride microresonators exhibiting low-power frequency comb initiation," *Optica* **3**(11), 1171–1180 (2016).
16. M. H. P. Pfeiffer, A. Kordts, V. Brasch, M. Zervas, M. Geiselman, J. D. Jost, and T. J. Kippenberg, "Photonic Damascene process for integrated high-Q microresonator based nonlinear photonics," *Optica* **3**(1), 20–25 (2016).
17. C. E. Morosanu, "The Preparation, Characterization and Applications of Silicon Nitride Thin Films," *Thin Solid Films* **65**(2), 171–208 (1980).
18. X. Cheng, J. Hong, A. M. Spring, and S. Yokoyama, "Fabrication of a high-Q factor ring resonator using LSCVD deposited Si<sub>3</sub>N<sub>4</sub> film," *Opt. Mater. Express* **7**(7), 2182–2187 (2017).
19. F. Ay and A. Aydinli, "Comparative investigation of hydrogen bonding in silicon based PECVD grown dielectrics for optical waveguides," *Opt. Mater.* **26**(1), 33–46 (2004).
20. J. S. Levy, A. Gondarenko, M. A. Foster, A. C. Turner-Foster, A. L. Gaeta, and M. Lipson, "CMOS-compatible multiple-wavelength oscillator for on-chip optical interconnects," *Nat. Photonics* **4**(1), 37–40 (2010).
21. J. P. Epping, M. Hoekman, R. Mateman, A. Leinse, R. G. Heideman, A. van Rees, P. J. M. van der Slot, C. J. Lee, and K.-J. Boller, "High confinement, high yield Si<sub>3</sub>N<sub>4</sub> waveguides for nonlinear optical applications," *Opt. Express* **23**(2), 642–648 (2015).
22. Y. Huang, Q. Zhao, L. Kamyab, A. Rostami, F. Capolino, and O. Boyraz, "Sub-micron silicon nitride waveguide fabrication using conventional optical lithography," *Opt. Express* **23**(5), 6780–6786 (2015).
23. M. Shaw, J. Guo, G. A. Vawter, S. Habermehl, and C. Sullivan, "Fabrication techniques for low loss silicon nitride waveguides," *Proc. SPIE* **5720**, 109–118 (2005).
24. K. Wörhoff, A. Driessen, P. V. Lambeck, L. T. H. Hilderink, P. W. C. Linders, and T. J. A. Popma, "Plasma enhanced chemical vapor deposition silicon oxynitride optimized for application in integrated optics," *Sens. Actuat. Phys.* **74**(1–3), 9–12 (1999).
25. W. Xie, Y. Zhu, T. Aubert, S. Verstuyft, Z. Hens, and D. Van Thourhout, "Low-loss silicon nitride waveguide hybridly integrated with colloidal quantum dots," *Opt. Express* **23**(9), 12152–12160 (2015).
26. G. P. Agrawal, *Nonlinear Fiber Optics* (Academic, 1995).
27. T. Han, S. Madden, S. Debarma, and B. Luther-Davies, "Improved method for hot embossing As<sub>2</sub>S<sub>3</sub> waveguides employing a thermally stable chalcogenide coating," *Opt. Express* **19**(25), 25447–25453 (2011).
28. C. J. Krückel, A. Fülöp, T. Klintberg, J. Bengtsson, P. A. Andrekson, and V. Torres-Company, "Linear and nonlinear characterization of low-stress high-confinement silicon-rich nitride waveguides," *Opt. Express* **23**(20), 25827–25837 (2015).
29. X. Liu, M. Pu, B. Zhou, C. J. Krückel, A. Fülöp, V. Torres-Company, and M. Bache, "Octave-spanning supercontinuum generation in a silicon-rich nitride waveguide," *Opt. Lett.* **41**(12), 2719–2722 (2016).
30. M.-C. Tien, J. F. Bauters, M. J. R. Heck, D. J. Blumenthal, and J. E. Bowers, "Ultra-low loss Si<sub>3</sub>N<sub>4</sub> waveguides with low nonlinearity and high power handling capability," *Opt. Express* **18**(23), 23562–23568 (2010).

## 1. Introduction

Recently, silicon nitride (SiN) has become more and more attractive as an important alternative to silicon for integrated nonlinear optical applications [1–4]. By using silicon dioxide as a buffer layer underneath, SiN optical waveguide could possess the same benefits provided by SOI (silicon-on-insulator) counterparts [5,6]. The relatively large index contrast between SiN and silicon dioxide still allows high confinement of optical modes in SiN waveguides, which enables strong light-matter interaction and compact planar photonic circuits as well. Compared with silicon, the transparency window of SiN can be extended from visible to near infrared wavelengths of the C-band. Additionally, it has a considerably high Kerr nonlinearity, while does not suffer from the large TPA (two-photon absorption) effects at telecommunication wavelengths [7–9]. The low propagation loss combining with the advantages mentioned above makes SiN photonics a great platform in nonlinear optics application such as wavelength conversion, super-continuum generation, frequency comb generation and so on [1,10–13].

To obtain optical devices with good performances both in linear or nonlinear regime, SiN film with high quality is firstly required. Usually it can be deposited either by low pressure chemical vapor deposition (LPCVD) or by plasma-enhanced chemical vapor deposition (PECVD). LPCVD can provide SiN film with good homogeneity both in thickness and material quality. However, it involves high deposition temperature (in general 700-900 °C) and its growth rate is rather low. Because of the increasing tensile stress during deposition, the thickness of the film that can be deposited via LPCVD is limited to be ~400 nm, beyond which cracks would happen. The limited thickness imposes big challenge for subsequent waveguide dispersion engineering. Deep trenches have been adopted to overcome this stress limitation on LPCVD platform [14–16], with the cost of adding processing complexity. In contrast to expensive LPCVD, low-cost PECVD facility is often more readily available. A crack-free SiN film with thickness up to 1.0  $\mu\text{m}$  can be easily grown by PECVD at a much higher deposit rate under a lower deposition temperature [17]. The problem for the SiN film prepared by PECVD (usually with a gas mixture of  $\text{SiH}_4$ ,  $\text{NH}_3$  and  $\text{N}_2$ ) is it always has relatively large intrinsic absorption loss due to the dangling bonds of Si-H and N-H, which is formed during the deposition [18,19]. So far, many SiN based nonlinear optical waveguides have been proposed, but most of them are obtained from LPCVD [7,12,20–22,28,30]. SiN waveguides grown by PECVD which have a similar optical linear and nonlinear performance are still rarely seen. In addition, for the fabrication of the SiN optical waveguides, it is noticed that most of them are realized by high resolution but expensive lithography, such as E-beam or DUV (deep-ultraviolet). It is very desirable if the highly accessible conventional UV contact lithography can be utilized to fabricate these waveguides [22]. The device fabrication area and waveguide length could easily be scaled up with this fabrication method, which is not achievable for those high resolution methods.

In this work, we present a nonlinear SiN optical waveguide. These waveguides are fabricated by readily available PECVD, conventional contact UV-lithography and high-temperature annealing techniques, thus dramatically reducing the processing complexity and cost. It is found that by patterning the waveguide structures firstly and then carrying out a high-temperature annealing process [23,24], not only sufficient waveguide thickness can be achieved, which gives more freedom to waveguide dispersion control, but also the material absorption loss in the waveguides be greatly reduced. The linear optical loss of the fabricated waveguide with a cross-section of  $2.0 \times 0.58 \mu\text{m}^2$  was measured to be as low as 0.58 dB/cm. And the same loss level is demonstrated over a broad wavelength range from 1500 nm to 1630 nm. Moreover, the nonlinear refractive index of the waveguide was determined to be  $\sim 6.94 \times 10^{-19} \text{ m}^2/\text{W}$ , indicating that comparable nonlinear performance with their LPCVD counterparts is expected. The proposed fabrication process provides a feasible and promising alternative for the development of on-chip nonlinear optical devices or circuits using SiN photonics by PECVD deposition platform.

## 2. Waveguide fabrication

We fabricated SiN waveguides using contact lithography and the designed pattern consists of waveguides with widths varying from 0.8  $\mu\text{m}$  to 2.0  $\mu\text{m}$ , each of which has a straight reference waveguide and spiral waveguides with a set of lengths 1, 2, 4, and 8 cm for cut-back measurements. To have negligible bending loss, the bend radius of the spiral part is fixed at 100  $\mu\text{m}$ , according to a numerical simulation. The fabrication process of the SiN waveguide is schematically shown in Fig. 1. Firstly, the SiN layer was deposited at a desired film thickness by PECVD on a 4 inch silicon substrate with a 5  $\mu\text{m}$  oxide box layer, which was obtained by wet thermal oxidation method. The gases used for deposition are a mixture of 5%  $\text{SiH}_4$  diluted by  $\text{N}_2$  (600 sccm) and pure  $\text{NH}_3$  (16 sccm). The process temperature was set at 400°C, and the process pressure is 1200 mTorr. The plasma frequencies were alternated between a high frequency (13.56 MHz) and a low frequency (100 kHz), both with a power of 50 W. The time duration for the two frequencies are 13 seconds and 7 seconds, respectively.

The above optimized deposition parameters can guarantee SiN film with good optical quality and uniformity. The refractive index of the deposited film was measured by ellipsometry to be 2.01 at 1550 nm wavelength. In the next step, a layer of positive photoresist with a thickness of 800 nm was spin coated on the wafer and cured. A high quality contact mask was used in combination with a contact mask aligner (MA6, Karl Suss) to define the pattern of waveguide structures. The intensity of i-line source on the mask aligner is  $5.0 \text{ mW/cm}^2$ . Then, after the development and hard-bake process, reactive ion etching (RIE) was used to transfer the pattern of the photoresist into the SiN layer, forming the waveguide core structure. The etching gases were chosen to be a mixture of  $\text{CF}_4$  and  $\text{H}_2$ , with a flow ratio of 80 sccm to 3 sccm. The plasma power was set to be 210 W and a chamber pressure be 20 mTorr [25]. With the optimized etching process, strip SiN waveguides with steep and smooth sidewalls were obtained, which is shown in Fig. 2, together with a microscope image of a 4 cm long spiral waveguide. After waveguide etching, the photoresist was removed by acetone and further cleaned by  $\text{O}_2$  plasma. An oxide top cladding with thickness of  $3 \mu\text{m}$  can be selectively deposited, also by PECVD, for the waveguide protection or metal deposition.

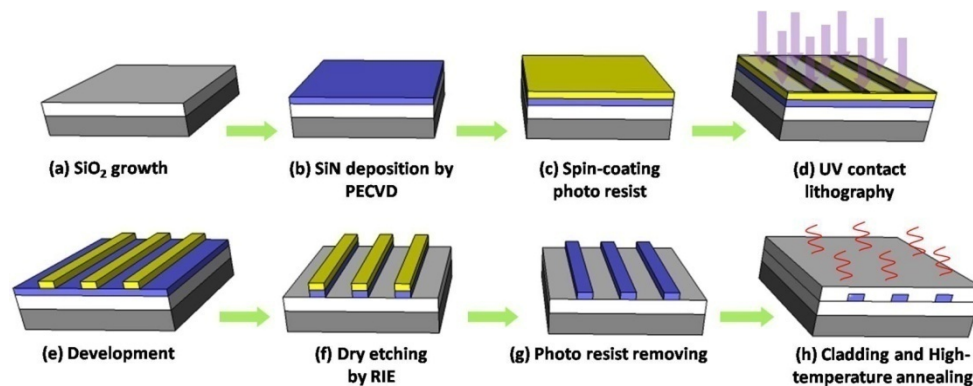


Fig. 1. The schematic picture of the fabrication processes of the SiN optical waveguide.

In our experiment, an extra high-temperature annealing step was carried out to reduce the intrinsic material absorption loss in SiN waveguides. During this process, the temperature of the annealing furnace filled with  $\text{N}_2$  gas was risen from  $300 \text{ }^\circ\text{C}$  to  $1150 \text{ }^\circ\text{C}$  with a rate of  $5 \text{ }^\circ\text{C/min}$ . At this temperature, the flowing gas was switched to  $\text{O}_2$  for half an hour, and then back to  $\text{N}_2$  atmosphere protection. The  $1150 \text{ }^\circ\text{C}$  annealing process lasted for about 3 hours before the furnace temperature was dropped down to  $300 \text{ }^\circ\text{C}$  with a rate of  $3 \text{ }^\circ\text{C/min}$ . We note that all of the waveguides are intact without any defects or cracks after the annealing step. In contrast, the cracking always occurs when annealing as-deposited SiN layer without patterning. This can be explained by the fact that the annealing induced inner stress is hard to release in a large area compared with a patterned layer. So in general, more readily available PECVD with annealing can provide an feasible and promising alternative for obtaining high quality SiN waveguides with both sufficient thickness and low intrinsic material absorption loss, instead of resorting to LPCVD and adding extra process complexity.

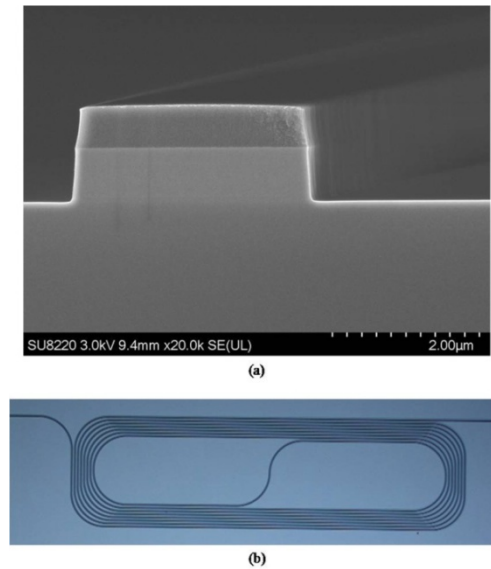


Fig. 2. (a) SEM image of the SiN waveguide (after dry etching, with photo resist on top); (b) Microscopic image of a 4 cm long spiral SiN waveguide.

### 3. Linear loss of the fabricated SiN waveguides

The linear optical loss of the fabricated SiN waveguides at 1550 nm telecommunication window are determined by the cut-back method. The waveguides under test were cleaved at both sides for butt coupling. The light from a tunable laser was tuned into TE polarization and coupled into one waveguide facet via a lensed fiber horizontally, and the transmitted light out from the other facet was collected through another lensed fiber and measured by an optical power meter. The transmission spectra of the waveguides with different lengths were acquired by sweeping the tunable laser from 1510 nm to 1630 nm. By comparison with the transmission spectra of the fabricated waveguides before annealing, the effect of the high-temperature annealing process on the material absorption of PECVD SiN was clearly evaluated. The linear optical losses at different wavelengths were also extracted, by fitting the length-dependent fiber-to-fiber transmission.

Figure 3(a) shows the measurement results of a set of waveguides as fabricated without annealing. The waveguides are with a cross-section of  $1.2 \times 0.58 \mu\text{m}^2$ . According to numerical simulation, only fundamental TE and TM mode are supported by such waveguide dimension, and our loss measurement was done under TE polarization. As can be seen, there is a distinct intrinsic absorption band centered at around 1525 nm, especially in longer spiral waveguides. The absorption band extends as far as to 1595 nm, with a bandwidth of more than 70 nm. This absorption band is attributed to the second overtone absorption of the N-H stretching vibration [19,24]. By linear fitting as shown in Fig. 3(b), the optical losses of the waveguides are determined to be 5.99 dB/cm, 4.99 dB/cm and 2.63 dB/cm at the wavelengths of 1525 nm, 1550 nm and 1600 nm, respectively. The small discrepancy between the measured and fitted results clearly demonstrates the reliability of the cut-back method for determining the waveguide loss. Since except for material loss the other loss contributions to waveguide total loss weakly depend on the wavelength, the difference of waveguides loss at different wavelengths is mainly due to material loss. Therefore, by comparing the loss value at 1525 nm and 1600 nm, the material absorption loss is thus evaluated to be 3.36 dB/cm in our SiN waveguides.

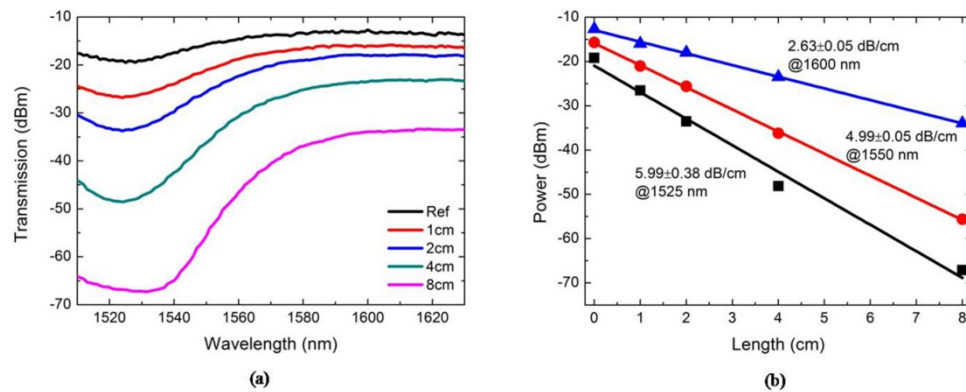


Fig. 3. (a) The optical transmission spectra of the fabricated SiN waveguide (with air top cladding, before high-temperature annealing); (b) Total waveguide losses at different wavelength determined with cut-back method.

To eliminate this material loss due to N-H bonds, a high-temperature annealing usually above 1000 °C is necessary to break down N-H bonds and release H in SiN film [19,24]. In our experiment, first we deposited a silicon oxide cladding layer with a thickness of 3 μm on top of those as-fabricated waveguides, and then carried out the high-temperature annealing process as mentioned before. After annealing, all of the waveguides were intact without any defects or cracks. We measured the transmission spectra again and the result is shown in Fig. 4(a). It is clearly seen that the absorption band centered at 1525 nm almost disappeared, resulting in dramatically reduced total waveguide loss at this wavelength. As shown in Fig. 4(b), the optical losses of the waveguides with 1.2 μm width were measured to be 1.29 dB/cm, 1.27 dB/cm and 1.08 dB/cm at the wavelengths of 1525 nm, 1550 nm and 1600 nm, respectively. Compared with the pre-annealing result, the loss difference at 1525 nm and 1600 nm is reduced from 3.36 dB/cm to 0.21 dB/cm of the post-annealing result, which implies that the material absorption loss was almost eliminated by our annealing process.

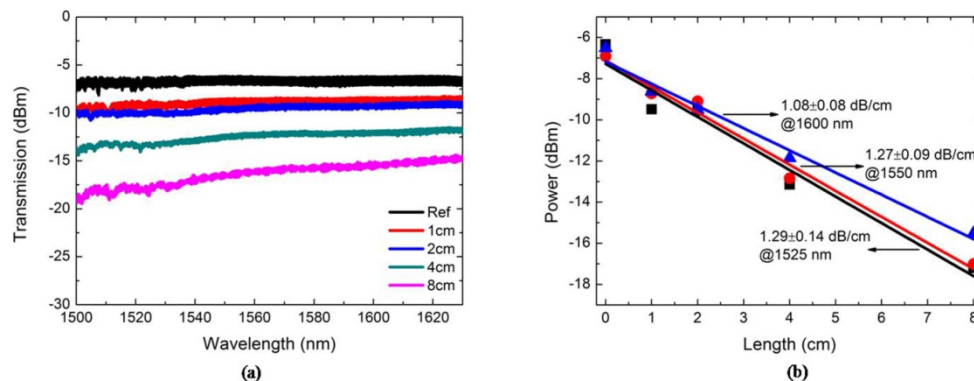


Fig. 4. (a) The optical transmission spectra of the fabricated SiN waveguide (with SiO<sub>2</sub> top cladding, after high-temperature annealing); (b) Total waveguide losses at different wavelength determined with cut-back method.

Note that the remaining small loss difference at different wavelengths can be from wavelength dependent scattering loss. In addition to material loss, the waveguide loss at non-absorption band, for example at 1600 nm, was also reduced by 1.55 dB/cm after annealing, compared with as-fabricated result. This loss reduction can be attributed to the SiO<sub>2</sub> cladding which lowers refractive index contrast between interfaces of SiN waveguide core and cladding and thus reduces scattering loss. Moreover, it is noted that there is no additional

material loss during SiO<sub>2</sub> deposition and annealing. The waveguide loss can be further reduced by increasing the width of waveguide and therefore suppressing scattering loss caused by sidewall roughness. In Fig. 5, we present the waveguide loss at 1550 nm as a function of waveguide width, which shows typical exponential relationship. From the simulated mode profile and confinement factor, it can be seen that due to our sufficient waveguide thickness by PECVD deposition, the mode is tightly confined within the waveguide with less overlap with the waveguide boundary [14]. Thus for 2.0 μm waveguide width, 0.58 dB/cm loss was achieved. In Table 1, these loss values are compared with current state-of-the-art realized on different platforms, which are oriented for nonlinear applications. It can be seen that with similar waveguide dimensions, linear loss level of these SiN waveguides has been pushed close to that of those by LPCVD, while not resorting to expensive DUV (deep-ultraviolet) or e-beam lithography method, as in Ref [8] and Ref [28]. The later is needed when the waveguide width falls below 1.0 μm, where scattering due to waveguide interfaces becomes dominant.

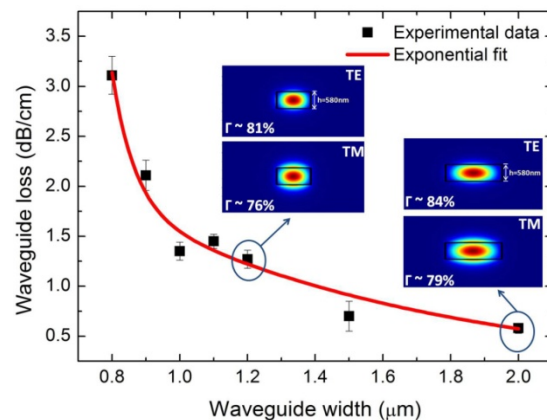


Fig. 5. Total optical losses for different waveguide width at 1550 nm. Insets show simulated mode profile of the waveguide and its confinement factor with different polarization.

#### 4. Optical nonlinearity of the fabricated SiN waveguides

In order to assess the performance of the optical nonlinearity of our fabricated waveguide, FWM (four-wave mixing) method with two continuous wave (CW) lasers was adopted. The experimental layout is shown in Fig. 6. The light output from two CW laser sources are both amplified by EDFA (erbium-doped fiber amplifiers) and used as pump and signal. A 3 dB coupler was used to combine the pump and signal together before they are coupled into the waveguide under test. Two polarization controllers were used to adjust the polarization states of pump and signal. The input power at the pump was monitored by a power meter, while the output spectrum was acquired using an optical spectrum analyzer. The conversion efficiency was determined by dividing the power of the generated idler waves with power of the signal.

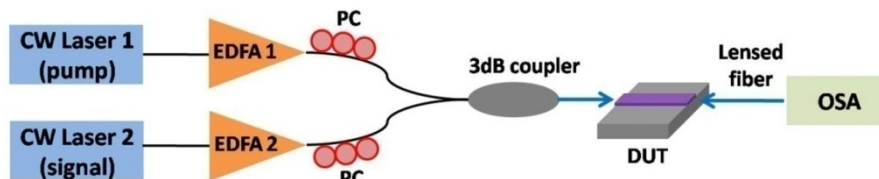


Fig. 6. The schematic picture of the FWM measurement setup.

The existence of the third order optical nonlinearity was firstly confirmed by the observation of the FWM phenomenon, as shown in Fig. 7. The waveguide thickness was

chosen to be 720 nm to meet the phase matching condition requirement, while the width was kept at 2.0  $\mu\text{m}$ . The length of the waveguide under measurement is 2.2 cm. When the pump wavelength centered at 1550 nm and signal wavelength centered 1550.8 nm, two idlers were clearly found at the wavelength of 1549.1 nm and 1551.6 nm. In this case, the output power from two EDFAs used as pump and signal are 31 dBm and 29.4 dBm. It has to be noted that the high powers used here were due to the relatively large coupling loss of the fiber to waveguide facets ( $\sim 9$  dB/facet). This certainly can be improved in the future by polishing the waveguide facets and introducing anti-reflection coating.

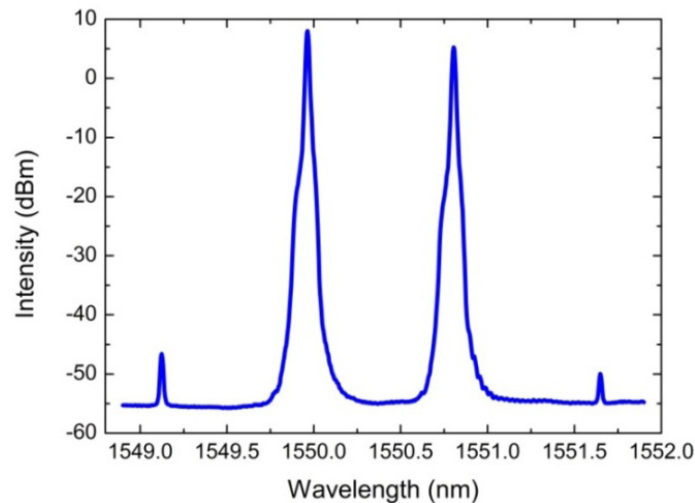


Fig. 7. Experimental FWM phenomenon observed with pump and signal at 1550 nm and 1550.8 nm, respectively.

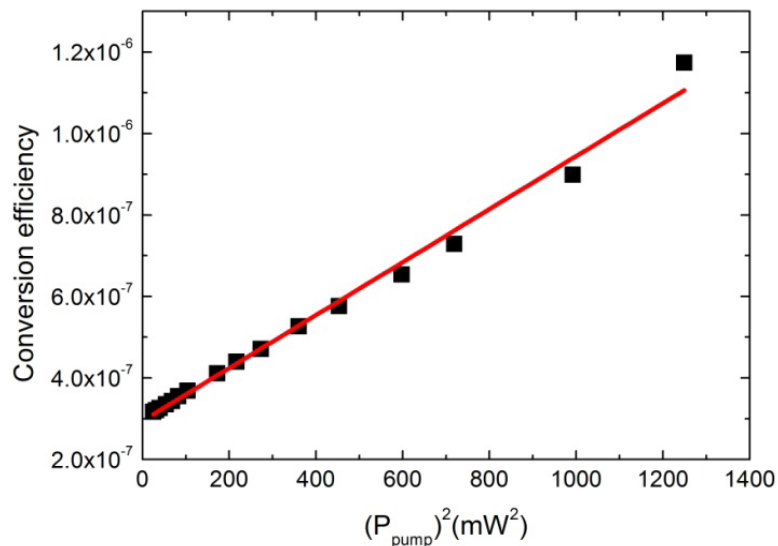


Fig. 8. The relationship between the conversion efficiency and the square of the input pump power.

Then, the nonlinear coefficient was quantitatively measured by varying the pump power while fixing the signal power at 29.4 dBm. Considering the coupling loss of the fiber to the waveguide as well as the total loss in the circuit link, the relationship between the conversion efficiency and the square of the pump power is plotted in Fig. 8. As can be seen, they are in

good agreement with a linear fit, which meets the theoretical prediction. The nonlinear coefficient can be calculated by using the following formula [26,27]:

$$\eta = \frac{P_i(L)}{P_s(0)} = (\gamma P_p L_{eff})^2 e^{-\alpha L} \quad (1)$$

where  $\eta$  is the idler conversion efficiency at the output,  $P_i(L)$  is the idler power,  $P_s(0)$  is the signal power at the input,  $P_p$  is the input power,  $\alpha$  is the linear propagation loss, and  $L_{eff}$  is the effective length, which is approximated by  $(1 - e^{-\alpha L})/\alpha$ . By using the linear optical loss value measured by cut-back method, the nonlinear coefficient was calculated to be  $2.62 \text{ W}^{-1} \cdot \text{m}^{-1}$ . The effective area of the fundamental mode  $A_{eff}$  was calculated by mode solver and is  $\sim 1.07 \text{ } \mu\text{m}^2$ , thus the nonlinear refractive index value  $n_2$  was estimated to be  $6.94 \times 10^{-19} \text{ m}^2/\text{W}$ , with the equation of  $n_2 = c \cdot \gamma \cdot A_{eff} / \omega$ . The value is comparable with that in LPCVD ones [3,4,28–30]. As seen in Table 1, the  $n_2$  value of our material falls in between the two reported ones in Ref [28] and Ref [3]. This accordance is expected as the bandgap energy of our material ( $\sim 3.27 \text{ eV}$ ) also falls in between the values of  $2.3 \text{ eV}$  and  $5.0 \text{ eV}$  reported in those literatures. The silicon-rich property of our material was further confirmed by the X-ray photoelectron spectroscopy measurement. The deposition recipe we used results in around 51.2% of Si content, which is higher than that of 43% in stoichiometric SiN film.

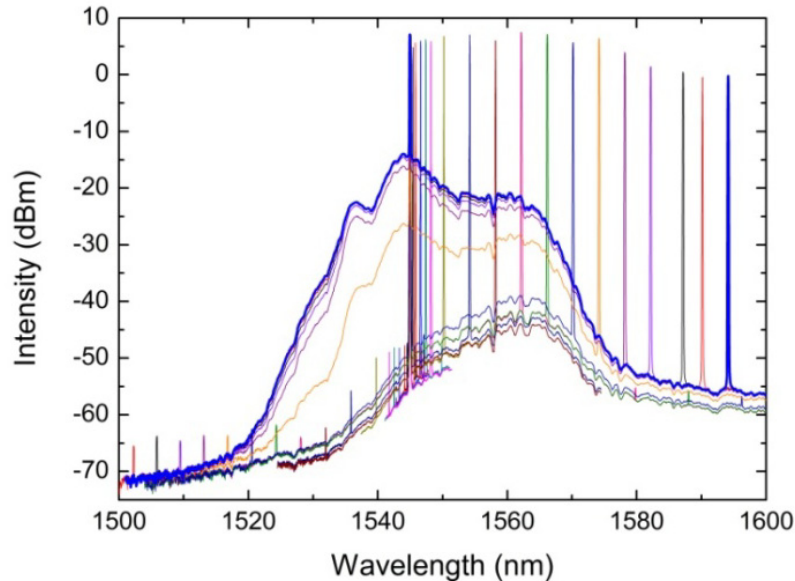


Fig. 9. Experimental FWM phenomenon between the wavelength of 1500 nm and 1600 nm.

Finally, we fixed the pump wavelength at 1545 nm with a setting power of 29.8 dBm and varied the wavelength of the signal, which has a power of 29.4 dBm. The result is shown in Fig. 9. As can be seen, the FWM was realized within a large wavelength range when the pump wavelength was properly chosen. The nearly 10 dB extinction ratio of the idler wave is adequate for the signal processing application in the C-band and L-band. Currently, we are working towards the more complicated optical devices (e.g. micro-ring resonator) using the same developed fabrication technology.

**Table 1. Comparison of our work with previous publications**

SiN Deposition method	Waveguide dimensions	Propagation loss	Polarization	$n_2$
PECVD (our work)	w = 1.2~2.0 $\mu\text{m}$ , h = 580 nm	0.58~1.27 dB/cm @1550 nm	TE	$6.94 \cdot 10^{-19}$
PECVD [3]	w = 1.0 $\mu\text{m}$ , h = 500 nm	4.0 dB/cm @1550 nm	TE	$2.4 \cdot 10^{-19}$
PECVD [8]	w = 1.0~1.5 $\mu\text{m}$ , h = 300 nm	1.5 dB/cm @1550 nm	TE	$2.3 \cdot 10^{-19}$ ~ $2 \cdot 10^{-18}$
LPCVD [20]	w = 1.5 $\mu\text{m}$ , h = 725 nm	0.5 dB/cm @1550 nm	TE	$1.1 \cdot 10^{-19}$
LPCVD [21]	w = 0.7~0.9 $\mu\text{m}$ , h = 800~1200 nm	0.37~1.37dB/cm @1560 nm	TM	-
LPCVD [22]	w = 0.8 $\mu\text{m}$ , h = 900 nm	$0.8 \pm 0.26$ dB/cm @1550 nm	TM	$1.39 \cdot 10^{-19}$
LPCVD [28]	w = 1.65 $\mu\text{m}$ , h = 700 nm	1.2 dB/cm @1570 nm	TE	$1.4 \cdot 10^{-18}$
LPCVD [30]	w = 2.8 $\mu\text{m}$ , h = 80 nm	0.03 dB/cm @1550 nm	TE	$9 \cdot 10^{-20}$

## 5. Conclusion

In conclusion, we demonstrate a nonlinear SiN waveguide. These waveguide are fabricated by readily available PECVD, conventional contact UV-lithography and high-temperature annealing techniques, which dramatically reduces the processing complexity and cost. The developed and optimized processes, can be utilized as an feasible and promising alternative to fabricate SiN waveguides with sufficient thickness, which allows more freedom on dispersion engineering in nonlinear applications. The important effect of high-temperature annealing in reducing the losses of SiN waveguide by PECVD is investigated experimentally. The fabricated waveguides by our process exhibit not only very low linear optical loss, but also considerable third-order optical nonlinearity, which is comparable with that in the LPCVD counterparts. These nonlinear SiN waveguides by PECVD deposition platform can be useful for the development of more complicated on-chip nonlinear optical devices or circuits.

## Funding

National Natural Science Foundation of China (NSFC) (61405198); Natural Science Foundation of Fujian Province (2017J01756).